Journal of Atmospheric and Solar–Terrestrial Physics 220 (2021) 105663

Contents lists available at ScienceDirect

Journal of Atmospheric and Solar-Terrestrial Physics

journal homepage: www.elsevier.com/locate/jastp

An experimental investigation into the possible connections between the zonal neutral wind speeds and equatorial plasma bubble drift velocities over the African equatorial region

D.I. Okoh [a,b,*], A.B. Rabiu [a,b], K. Shiokawa [c], Y. Otsuka [c], Q. Wu [d], G.K. Seemala [e], Z. T. Katamzi-Joseph [f]

[a] *Centre for Atmospheric Research, National Space Research and Development Agency, Anyigba, Nigeria*
[b] *Institute for Space Science and Engineering, African University of Science and Technology, Abuja, Nigeria*
[c] *Institute for Space-Earth Environmental Research, Nagoya University, Nagoya, Japan*
[d] *National Center for Atmospheric Research, High Altitude Observatory, Boulder, USA*
[e] *Indian Institute of Geomagnetism, Navi Mumbai, India*
[f] *South African National Space Agency, Space Science, Hermanus, South Africa*

A R T I C L E I N F O

Keywords:
Neutral wind
Plasma bubble
Zonal speed
Airglow
FPI
All-sky imager

A B S T R A C T

There is increasing interest to understand thermospheric neutral wind and ionized plasma coupling, especially by using empirical observations. This is the first study that reports simultaneous measurements of thermospheric neutral wind and equatorial plasma bubble (EPB) speeds over the African equatorial region. Neutral wind speeds were obtained using a Fabry-Perot interferometer (FPI), while EPB speeds were obtained using an all-sky optical imager. Both instruments are co-located in Abuja (Geographic: 8.99°N, 7.38°E; Geomagnetic: 1.60°S). Data for 11 nights of coincident neutral wind and EPB speed observations were used. The neutral wind speeds were in the range of about −30 to 300 m/s, while EPB speeds were in the range of about 15–400 m/s. The speeds of both neutral winds and EPBs were generally observed to be faster during the early night hours and to slow down towards midnight. In some instances, the neutral wind and EPB speeds were comparable, an observation that is in agreement with full development of the F region dynamo. There were also instances in which the EPBs were faster or slower than the neutral winds. In one of the nights, a southward turning of the IMF-Bz was observed to cause a sudden increase in the EPB speed. For some nights, the neutral winds were faster than the EPBs during earlier hours of the nights, and the disparity reduced during the later hours of the nights. This was attributed to the possibility that the F region dynamo was yet to be fully developed during the earlier hours.

1. Introduction

Plasma bubbles are F-region depletions usually observed during post-sunset periods in the equatorial ionosphere. Events in the equatorial ionosphere, such as plasma bubbles, are known to be controlled by geometry of the Earth's magnetic field, and interactions that exist between plasma, electrodynamics, and the neutral atmosphere (Rishbeth 2000; Abdu 2005; Chapagain 2015). Previous studies indicate that the equatorial ionosphere and thermosphere constitute a coupled system that possesses peculiar characteristics as compared to other latitude regions of the Earth (Schunk and Sojka, 1996; Abdu 2005). Studying the relationships between motions of ionized and neutral atmospheric components in the equatorial ionosphere-thermosphere region is therefore crucial to understanding the dynamics of the region.

In recent times, there is growing interest to understand these coupling activities of the ionosphere-thermosphere region (Yigit et al., 2016; Chen et al., 2017; Sivakandan et al., 2019; Koucka et al., 2020). By employing the equation of the ideal gas law and the momentum equation for the thermosphere, Fagundes et al. (1996) used night-time thermospheric neutral wind measurements from a Fabry-Perot interferometer in Brazil to infer the motion of low-latitude plasma drifts in the F-region. They reported that their results were in reasonable agreement with those observed in other low-latitude locations, and that they sometimes observed that the winds flow from the observed coldest parts to the hottest parts of the thermosphere during many hours, leading them to the conclusion that plasma drift can drive the neutral

* Corresponding author. Centre for Atmospheric Research, National Space Research and Development Agency, Anyigba, Nigeria.;
E-mail address: okodan2003@gmail.com (D.I. Okoh).

https://doi.org/10.1016/j.jastp.2021.105663
Received 25 November 2020; Received in revised form 12 February 2021; Accepted 22 April 2021
Available online 14 May 2021
1364-6826/

winds at low latitudes for a period of time. Sarudin et al. (2019) used a high density network of GPS receivers over South-East Asia to derive plasma bubble zonal drift velocity, and compared the result with neutral wind velocity from a Fabry-Perot interferometer on the night of April 10, 2013. They obtained a maximum plasma bubble drift of about 194.4 m/s at around 22:00 LT, and a minimum drift of about 111.1 m/s at around 21:00 LT. Their results also show that the temporal variations of the plasma bubble drifts are consistent with the neutral winds.

Chapagain et al. (2013) used a one-year span of plasma bubble zonal velocity measurements and corresponding zonal neutral wind measurements to study relationship between the two velocities. Plasma bubble zonal velocity measurements were derived from OI 630.0 nm emission images recorded by a narrow-field optical imager in Chile, and the neutral wind measurements were obtained from Fabry-Perot interferometer in Peru. Their results show a generally good correlation between the zonal neutral winds and plasma bubble velocities. There are however cases where the plasma bubble velocities are different from the neutral winds, and they indicate that such differences could be due to the differences in apex altitudes for the plasma bubble velocity and neutral wind measurements. Fukushima et al. (2015) also compared zonal bubble velocities and zonal neutral wind velocities using geomagnetically conjugate measurements of 630.0-nm airglow at Thailand and Indonesia (~±10° magnetic latitudes). They concluded that the bubble drift velocities estimated from the thermospheric neutral winds measured at both hemispheres with considering ionospheric conductivities were 60–90% of the observed velocities of the plasma bubbles, suggesting that most of the plasma bubble velocity can be explained by the F region dynamo effect.

In the African equatorial region, there has not been a study on the relationship between plasma bubble velocity and neutral winds. Wiens et al. (2006) used an all-sky imager in Eritrea, East Africa, to monitor OI 630-nm nightglow for the nine months between September 2001 and May 2002. They found plasma bubbles on 63% of the nights with adequate viewing conditions, and they reported average near-midnight plasma bubble velocities of about 100–120 m/s. Using a Fabry-Perot interferometer in Ethiopia, still in East Africa, Tesema et al. (2017) separately reported measurements of equatorial thermospheric winds in the region. For about six-month period between November 2015 and April 2016, they obtained eastward maximum monthly-averaged zonal winds in the range of 70–90 m/s between 19:00 and 21:00 LT.

The study by Okoh et al. (2017) is the first report on observation of equatorial plasma bubbles using an all-sky optical imager in the West African equatorial region. The occurrence frequency of plasma bubbles was studied using 147 nights of clear-sky observations in the period from June 9, 2015 to January 31, 2017, and plasma bubbles were detected in 48% of the observations. A majority of the plasma bubbles were detected during the equinoxes than during the solstices, and the occurrence rate was highest around local midnight than during the hours farther away from midnight. Most of the post-midnight plasma bubbles were also observed around the months of December to March. The present study is the first report on the relationship between thermospheric neutral wind and plasma bubble speeds in the African equatorial region.

2. Data and methods

Data used in this work comprise of neutral wind speed measurements obtained from Fabry-Perot interferometer (FPI), and plasma bubble speed measurements obtained from an All-Sky Optical Imager. Both equipments are co-located at the Space Environment Research Laboratory (SERL), of the Centre for Atmospheric Research (CAR), within the premises of the National Space Research and Development Agency (NASRDA) Headquarters in Abuja, Nigeria. [Geographic: 8.99°N, 7.39°E; Geomagnetic: 1.60°S]. Data used in this work span the periods from year 2016–2017.

2.1. Neutral wind speed from FPI

For many years now, FPIs have been used to measure neutral wind speeds in the thermosphere. The FPI used in this work is developed by the National Center for Atmospheric Research (NCAR). It measures the Doppler shift in the O 630 nm airglow emission induced by the neutral wind, and from this measurement, the neutral wind speed is derived (Conde et al., 2001; Wu et al., 2004; Shiokawa et al., 2012; Xu et al., 2019).

The Abuja FPI has a rotating stage, with a mirror for viewing at an elevation angle of 45°. The rotating stage is used to drive the equipment to look in four azimuth directions (North, West, East, and South). The equipment was calibrated to ensure a pointing accuracy of 1°. The parts of the FPI under the rotating stage consist of a filter, an etalon, a lens, and a CCD camera. The etalon temperature is controlled by a temperature controller, which is set at 35 °C, and the CCD camera temperature is set at −8.5 °C. The Abuja FPI is connected to a cloud detector which monitors the sky condition. Information on the sky condition from the cloud detector is recorded to the data header, and it is used for data selection. Cloud cover foils accurate observations of airglow emissions from the ground, and so periods of cloud cover are removed from the observations.

The integration time is 10 min, and the recorded images contain multiple orders of the 630.0 nm emission spectra collected by the FPI. The orders are analyzed individually to estimate information on the Doppler shift. The individual estimates obtained from each order are then averaged together, and weighted by the uncertainty of the individual estimates to obtain the final values used. A zero reference for the Doppler shifts is established to obtain absolute estimates of the line-of-sight neutral wind (Wu et al., 2004; Makela et al., 2011).

Data recorded by the FPI are stored as images. Each image format is 346x258 pixels of 2-byte unsigned integers, which are results of 4x4 binning of the CCD chip. For the purpose of this work, the images are processed into wind speed information using software developed at NCAR. Wu et al. (2004) describes details of the processes involved.

2.2. Plasma bubble speed from all-sky optical imager

Plasma bubble speeds were obtained from the All-Sky Optical Imager No. 5 of the Optical Mesosphere Thermosphere Imagers (OMTIs). The OMTIs are provided by the Institute for Space-Earth Environmental Research (ISEE), Nagoya University. The imager has a 180° solid angle field of view, and it is operated with five filters in the following wavelength bands: 557.7 nm, 630.0 nm, 720–910 nm, 777.4 nm, and 572.5 nm. Images of the 630.0 nm filter were used in this study. The exposure time for this filter is 165 s. The all-sky image format is 512 × 512 pixels of 2-byte unsigned integers. The paper by Shiokawa et al. (2009) contains more information on the all-sky imager.

The images were first processed to enhance visibility of plasma bubble structures on them. To do this, we first constructed the percentage deviation images (I_{pd}) by using the formula in equation (1).

$$I_{pd} = \frac{I - I_{ra}}{I_{ra}} \times 100 \quad [\%] \tag{1}$$

I is the airglow intensity (in counts) of the raw image, and I_{ra} is the 1-h running average of the images. We then visually inspected the percentage deviation images to identify whether or not they contain plasma bubbles. To classify a structure as plasma bubble, we made sure that the amplitude of the structure was greater than 1%. Samples of the percentage deviation images which contain plasma bubbles (for the night of October 20, 2017) are shown in Fig. 1(a), while Fig. 1(b) shows samples of the percentage deviation images which do not contain plasma bubbles (for the night of November 4, 2016).

We identified a total of 11 nights which had clear skies for reliable measurements and coincident observations of both plasma bubble and

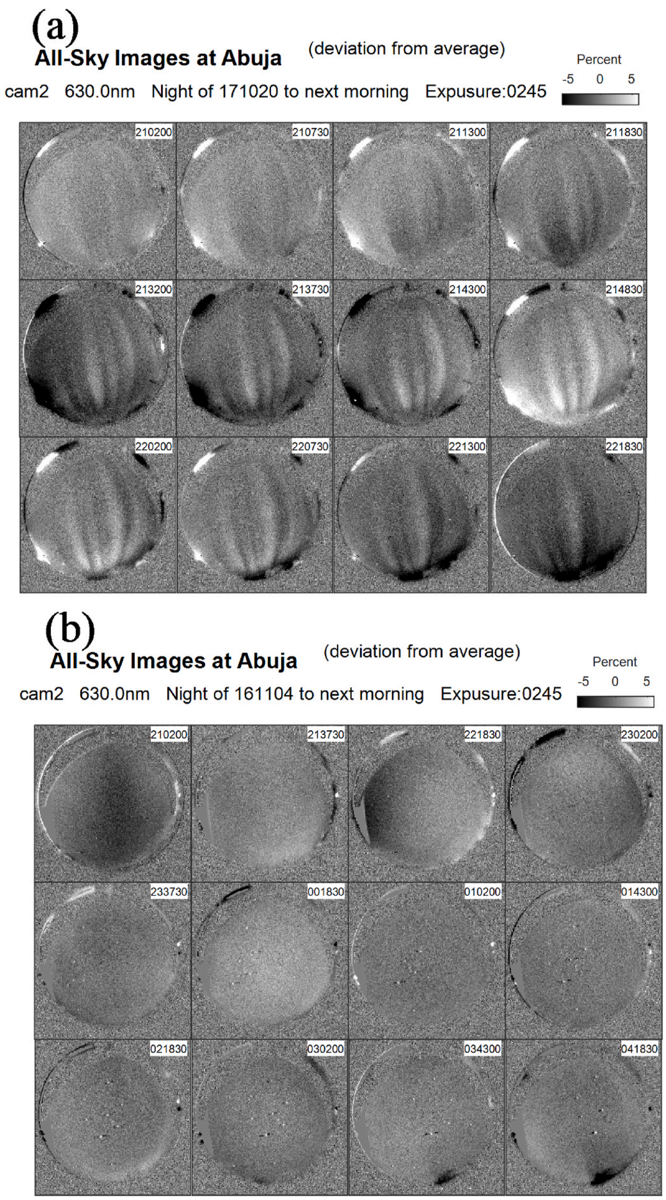

Fig. 1. Samples of percentage deviation images which: (a) contain plasma bubbles (for the night of October 20, 2017), (b) do not contain plasma bubbles (for the night of November 4, 2016).

neutral wind speeds. Table 1 is a summary of these nights. The last column of Table 1 contains information on the means of the amplitudes of the bubble structures for each of the nights.

Plasma bubble positions were identified as illustrated in Fig. 2, and these positions were consequently used to compute the plasma bubble speeds. The background images represent the spatially calibrated percentage deviation images from the all-sky imager. Only the image sections which are south of the all-sky imager location are shown. This is because the plasma bubbles were conspicuously observed in the lower half of the images; that is, south of the all-sky imager location (see Fig. 1 (a) for example). The East and West directions are as indicated on the figure. The red lines represent strips of the image pixel intensities (in the East-West direction), taken at a distance of 128 km from the top of the shown image. This is the strip along which the plasma bubble speeds were measured throughout this study. The red dots represent locations of the plasma bubble structures. Two plasma bubble structures can be seen on the images of Fig. 2, but we choose to illustrate with the eastward one. The plasma bubble positions correspond to the local minima of the red lines (that is, the darkest spots on the identified plasma bubble structures). Starting from earlier observations (at the top of Fig. 2) to later observations (at the bottom of Fig. 2), the plasma bubbles are observed to move in the eastward direction. The East-West directions indicated in Fig. 2 are the same East-West directions in which the images of the all-sky camera are recorded. We compute the plasma bubble speeds (S_p) using the formula in equation (2).

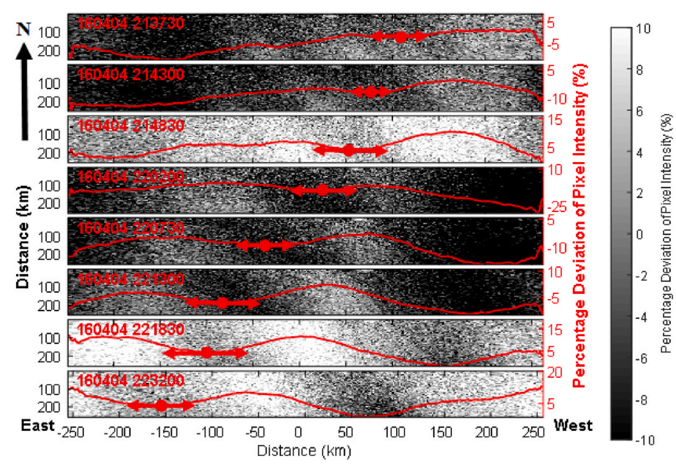

Fig. 2. Illustrating how plasma bubble positions were derived. The red dots indicate peak-intensity positions of the plasma bubbles, and the error bars indicate error estimates for those positions. Illustration is done using observations of April 4, 2016. The labels on the images are time stamps in the format: "yymmdd HHMMSS". (For interpretation of the references to colour in this figure legend, the reader is referred to the Web version of this article.)

Table 1
Observation nights studied in this work, for which there are clear skies for reliable measurements and coincident observations of both plasma bubble and neutral wind speeds.

Date	Kp		Dst (nT)		F10.7 (sfu)	Mean of structure amplitudes (%)
	Minimum	Maximum	Minimum	Maximum		
April 4, 2016	1.0	1.0	−19	−16	83.5	3.72
April 10, 2016	0.0	2.3	−9	−5	111.1	2.89
April 13, 2016	2.7	3.3	−34	−31	108.8	6.22
April 28, 2016	0.3	0.7	−3	3	96.3	1.46
May 1, 2016	3.7	3.7	−27	−19	93.6	3.77
June 2, 2016	0.3	1.0	−6	−3	87.7	5.42
June 3, 2016	0.3	0.7	−5	−1	85.7	6.36
June 22, 2016	1.7	3.3	−10	−3	80.9	1.68
October 20, 2017	1.3	1.7	−11	−2	75.1	4.31
November 15, 2017	2.0	2.3	−1	8	72.6	4,12
November 23, 2017	2.7	3.0	−8	−6	70.6	5.45

$$S_p = \frac{P_1 - P_2}{t_2 - t_1} \tag{2}$$

P_1 and P_2 are respectively positions of the plasma bubble (measured with respect to the distance scale on the horizontal axis) for observations recoded at times t_2 and t_1. An altitude of 250 km is assumed for the airglow layer.

The error in a given position (E_p) is estimated as the full-width at half-maximum of the curve profile around the identified peak. This is indicated by the width of the error bars shown in Fig. 2. Then, the error in a given speed is computed as: $E_s = (E_{p1} + E_{p2})/(2*(t_2 - t_1))$, where E_{p1} and E_{p2} are errors in the positions from which the speed is computed.

The plasma bubble speeds were first computed separately for different plasma bubbles identified on a given observation night. Then, the average of all plasma bubble speeds in an observation night were computed in bins of 15 min. For the purpose of uniformity, the neutral wind speeds obtained from the FPI measurements were also averaged in bins of 15 min. Fig. 3 contains the final plots of averaged neutral wind and plasma bubble speeds, binned in 15 min intervals.

3. Results and discussion

In Fig. 3, the measured neutral wind speeds are plotted alongside the measured plasma bubble speeds for the 11 observation nights when there are coincident observations of plasma bubbles and neutral winds. For the 11 observation nights investigated, it was found that the neutral wind speeds were in the range of about −30 to 300 m/s, while the plasma bubble speeds were in the range of about 15–400 m/s. The speeds of both neutral winds and plasma bubbles were generally observed to be faster during the early night hours and to slow down towards midnight.

In terms of comparison between the neutral wind and EPB speeds, the results from the 11 events can be grouped into the following 3 categories, and discussed in subsequent subsections.

Category 1: The EPB speeds and the neutral wind speeds are comparable (Fig. 3(a)–(d) which are for 160410, 160622, 171020, and 171123 respectively).

Category 2: The EPBs are faster than the neutral winds (Fig. 3(e)–(g) which are for 160413, 160428, and 171115 respectively).

Category 3: The EPBs are slower than the neutral winds (Fig. 3(h)–(k) which are for 160404, 160501, 160602, and 160603 respectively).

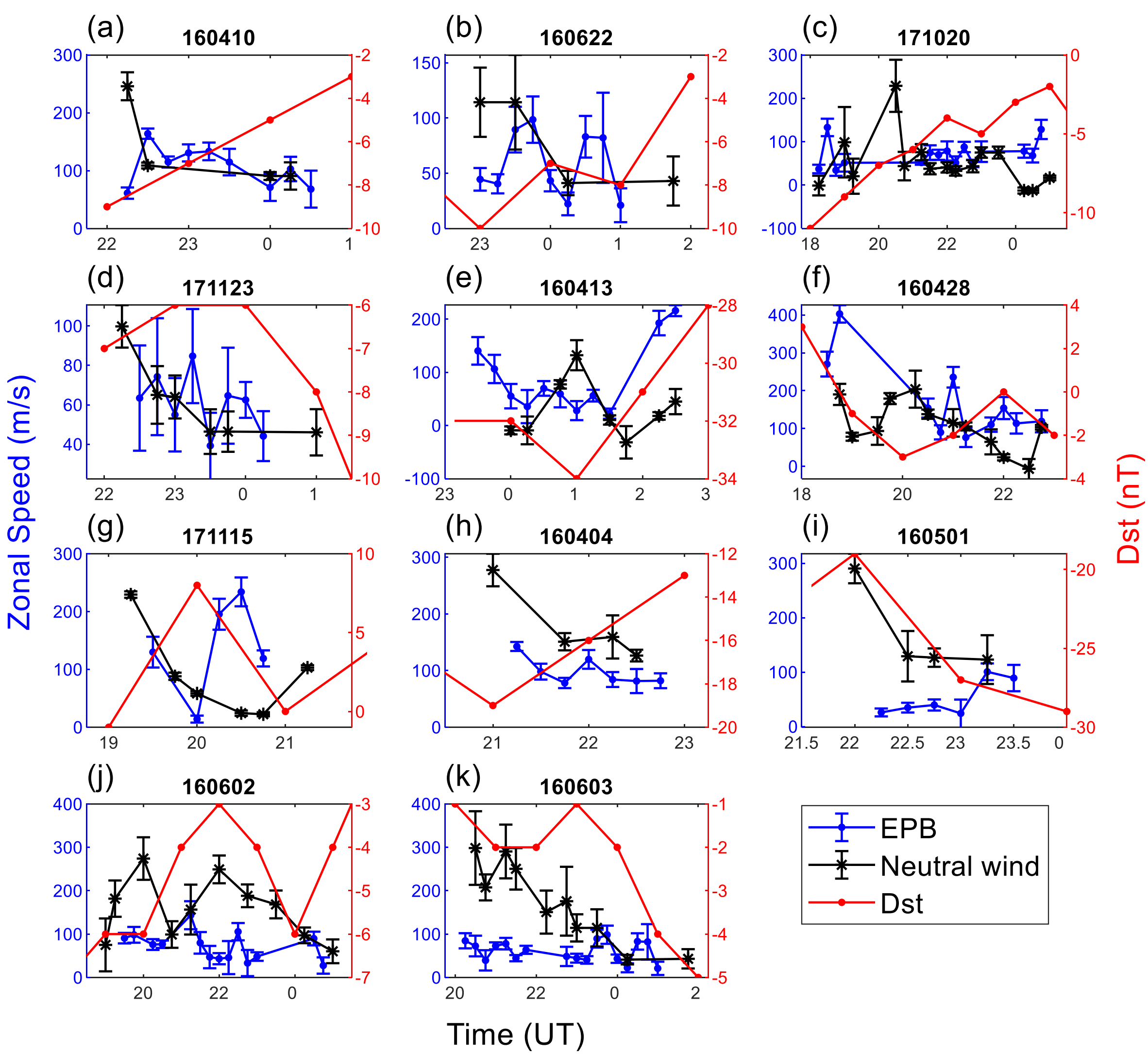

Fig. 3. Zonal speeds of the neutral winds and EPBs measured in Abuja. The plots are titled with dates of the observation nights in the format: “yymmdd”, where yy is the last 2 digits for the year, mm is 2 digits for the month, and dd is 2 digits for the day of the month. The left vertical axis denotes scale for the neutral wind and EPB speeds, the right vertical axis denotes scale for the Dst indices, and the horizontal axis denotes scale for the UT hour.

3.1. *Category 1 (The EPB speeds and the neutral wind speeds are comparable)*

The EPB speeds and the neutral wind speeds are observed to be comparable during the nights of 160410, 160622, 171020, and 171123. All of these four days were completely geomagnetic quiet days. The EPB and neutral wind speeds are typically expected to be comparable if the F-region dynamo is fully activated (Rishbeth, 1971a, 1971b; Chapagain et al., 2013; Fukushima et al., 2015). Rishbeth (1971a, 1971b) first introduced the idea of the F-region dynamo, and he explained that neutral winds blowing across magnetic field lines cause a slow transverse drift of the positive ions in a direction that is perpendicular to both the winds and the field lines. He further explained that this slow transverse drift sets up a polarization electric field which can only be neutralized by currents flowing along magnetic field lines and through the E-layer. However, the E-layer conductivity reduces significantly at night, and may become too small to close the circuit. In this case, the polarization electric field is not short-circuited in the E region, causing the plasma to drift with the wind (Rishbeth 1971b; Chapagain et al., 2013; Maute and Richmond, 2017). This is one reason why the EPB and neutral wind speeds could be comparable in those nights. Also, the ion drag force reduces the difference between the ion velocity and neutral wind velocity. The force on motions of neutral particles associated with electric currents tends to move the neutral particles toward the ion motions, thereby reducing the velocity difference between the ions and neutral particles (Akasofu and Dewitt, 1965; Maute and Richmond, 2017).

3.2. *Category 2 (The EPBs are faster than the neutral winds)*

The zonal drift speeds of EPBs are observed to be faster than the neutral winds during most of the nights of 160413, 160428, and 171115. One reason why the EPB speeds could be greater than the neutral wind speeds is that the altitude in which the EPBs are observed is higher than that in which the neutral winds are observed (e.g., Chapagain et al., 2013). This is however not the case in the present study, since the altitudes for all EPBs and all winds are expected to be the same, because they are measured using the same 630-nm airglow emission.

Magnetic activity can also affect EPB formation and their motion (e.g., Tulasi Ram et al., 2015; Sripathi et al., 2018). There was geomagnetic storm occurrence on the day of 160413 (with Dst index reaching −55 nT at 06:00 UT, and the values remained less than −30 nT for the rest of the day). There was a weak disturbance on 171115 (with Dst index reaching −29 nT at 09:00 UT). On 171115, the EPB and neutral wind speeds were particularly similar during the start of the observations until around 20:00 UT when there was a sudden increase in the EPB speed. The sudden increase in EPB speed coincides with southward turning of the IMF-Bz as shown in Fig. 4. As explained in section 3.3, previous researches show that geomagnetic storms typically cause decrease in eastward speeds of EPBs. Fig. 4 however reveals a contrasting scenario in which the sudden increase in the EPB speed coincides with the clearly evident southward turning of the IMF-Bz at around 20:00 UT.

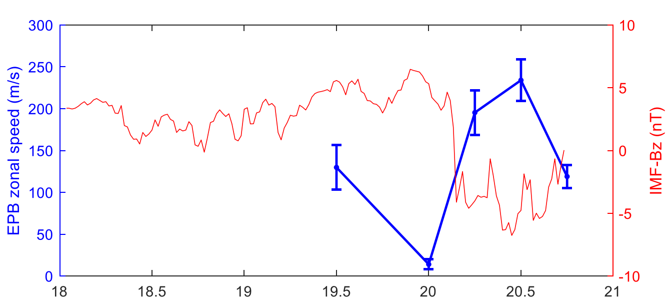

Fig. 4. Plots of the EPB zonal speed and IMF-Bz on 171115 showing sudden increase in the EPB speed and clear southward turning of the IMF-Bz at around 20:00 UT.

Fejer and Scherliess (1998), who have compared the zonal drift velocity observations from DE-2 satellite and from the Rice Convection Model, have shown that the sudden increase in the high-latitude convection induces prompt penetration of poleward/upward electric fields during nighttime, causing westward plasma drift. They have also shown that the penetration electric field decreases with decreasing latitudes. At the equator, the meridional component of the penetration electric field is smaller than the zonal component. The penetrations of intense eastward electric fields have also been reported by previous studies (e.g., Nishida, 1968; Kikuchi et al., 2000; Tulasi Ram et al., 2015; Sripathi et al., 2018). Previous studies (e.g., Fejer and Scherliess 1998) also show that the penetration electric fields have an upward component (causing westward ExB drift) during nighttime. This is opposite to the eastward drift enhancement shown in Fig. 4.

3.3. *Category 3 (The EPBs are slower than the neutral winds)*

The EPBs are observed to be slower than the neutral winds during most of the nights of 160404, 160501, 160602, and 160603. The night of 160404 came within the recovery phase of a geomagnetic storm that reached −56 nT at 00:00 UT of the previous day. The night of 160501 came within the commencement of a weak storm that reached −37 nT Dst at 04:00 UT of the following day. Geomagnetic storms are known to cause penetration and disturbance dynamo electric fields in the equatorial ionosphere, and this in turn changes the zonal drift of the background plasma and EPBs (Bhattacharyya et al., 2002; Huang et al., 2005, 2010; Huang and Roddy, 2016). The EPBs normally drift eastward during pre-midnight hours during magnetically quiet periods. However, under magnetic storm conditions, the EPB drifts typically reverse to westward (Abdu et al., 2003; Santos et al., 2016; de Paula et al., 2019). Huang and Roddy (2016) specifically observed that geomagnetic activities cause a decrease of the eastward drift velocity of plasma bubbles, equivalent to the occurrence of a westward drift, through disturbance dynamo process.

The other two days (160602 and 160603) were geomagnetic quiet days. Another reason why plasma bubbles may be slower than neutral winds is that the large horizontal pressure gradient in the early evening generates large neutral wind velocities in the evening to midnight period (Chapagain et al., 2012). This is prior to full development of the F-region dynamo. As the dynamo fully develops, the nighttime thermospheric neutral wind starts impacting plasma motion (e.g., Rishbeth, 1971b; Kelley, 1989; Park et al., 2010). The effect is that the differences between the neutral wind and EPB speeds are larger during the early hours and smaller during the later hours. This is due to the ion drag as the dynamo fully develops. This is the scenario that is predominantly observed in the four nights in which the EPBs are slower than the neutral winds. Similar observations are reported in the works of Chapagain et al. (2012) and Oberheide et al. (2015). Chapagain et al. (2012) specifically noted that the neutral wind speeds could be statistically larger than the EPB speeds for several hours, and that the difference between the neutral wind and EPB speeds could be up to 100 m/s. In the present study, it is observed that the difference between the neutral wind and EPB speeds get up to 200 m/s.

4. Conclusion

Results on simultaneous measurements of neutral wind and EPB speeds over the African equatorial region were presented. Neutral wind speeds were obtained using an FPI, while EPB speeds were obtained using an all-sky airglow imager which is co-located with the FPI in Abuja, Nigeria (Geographic: 8.99°N, 7.38°E; Geomagnetic: 1.60°S). Data for 11 nights of coincident neutral wind and plasma bubble speed observations were used.

For the 11 observation nights studied, the neutral wind speeds were in the range of about −30 to 300 m/s, while observed plasma bubble speeds were in the range of about 15–400 m/s. The speeds of both the neutral winds and plasma bubbles were generally observed to be faster during the early night hours and to slow down towards midnight. In some instances, the speeds of both the neutral winds and plasma bubbles were observed to be comparable. These were attributed to fully developed F region dynamos. There were also instances in which the EPBs were faster, and slower, than the neutral winds. The EPB eastward motion was particularly observed to become faster than the neutral wind at an instance of southward turning of the IMF-Bz. This eastward enhancement of the EPB motion is opposite to the directions observed in previous study by Fejer and Scherliess (1998). Slower EPB speeds occurring during geomagnetic storms were explained to probably be consequence of geomagnetic activity as explained in previous studies. The neutral winds were observed to be faster than the EPBs typically during the early hours of the evening, then later in the nights the neutral wind and EPB speeds converge. These observations were explained to be due to the large horizontal pressure gradient in the early evenings that generate large neutral wind speeds at those times, prior to full development of the F-region dynamo. The speeds converge as the F-region dynamo fully develops.

This is the first report on the relationship between thermospheric neutral wind and plasma bubble speeds in the African equatorial region. Past studies of the equatorial bubble motion and ion drift were mostly in the South American region, where the magnetic declination is different from that in the West African region. The magnetic declination affects the occurrences of the plasma bubble and ion-neutral interaction in the zonal and merdional directions. Knowledge of the atmospheric neutral-charged particle dynamics, especially for lesser studied areas like the African equatorial region, is important to increase understanding of space weather phenomena, and to develop or advance theories in the field. Results from the study particularly support the theory of the F-region dynamo, and that the neutral winds can be faster than the EPBs due to large horizontal pressure gradients in the early evenings, prior to full development of the dynamo. The enhancement of eastward EPB speed during southward turning of the IMF-Bz has not been previously reported in studies from other regions, and therefore opens a field of thought for possible theories.

Declaration of competing interest

The authors declare that they have no known competing financial interests or personal relationships that could have appeared to influence the work reported in this paper.

Acknowledgement

The airglow image data used in this work were obtained from the all-sky optical imager No. 5 of the Optical Mesosphere Thermosphere Imagers (OMTIs) provided by the Institute for Space-Earth Environmental Research (ISEE), Nagoya University. The data of the imager are available at https://ergsc.isee.nagoya-u.ac.jp/data_info/ground.shtml.en. The Fabry-Perot interferometer FPI installed in Abuja was deployed by the US National Center for Atmospheric Research (NCAR) with US National Science Foundation (NSF) based funding to NCAR and US Air Force Office of Scientific Research grant (FA9550-13-1-0174). Maintenance and operation of the all-sky optical imager No. 5 and FPI at the Space Environment Research Laboratory, Abuja has been supported by the Centre for Atmospheric Research using R & D fund from the Federal Government of Nigeria (www.carnasrda.com). Dst, Kp, F10.7, and IMF-Bz data were obtained from OMNIWeb (https://omniweb.gsfc.nasa.gov/form/dx1.html). This work has been supported by the Japan Society for the Promotion of Science (JSPS) core-to-core program (B: Asia-Africa Science Platforms).

References

Abdu, M.A., 2005. Equatorial ionosphere–thermosphere system: electrodynamics and irregularities. Adv. Space Res. 35, 771–787.

Abdu, M.A., Batista, I.S., Takahashi, H., MacDougall, J., Sobral, J.H.A., Medeiros, A.F., Trivedi, N.B., 2003. Magnetospheric disturbance induced equatorial plasma bubble development and dynamics: a case study in Brazilian sector. J. Geophys. Res. 108 (A12), 1449. https://doi.org/10.1029/2002JA009721.

Akasofu, S.I., Dewitt, R.N., 1965. Dynamo action in the ionosphere and motions of the magnetospheric plasma III. The Pedersen conductivity, generalized to take account of acceleration of the neutral gas. Planet. Space Sci. 13, 737.

Bhattacharyya, A., Basu, S., Groves, K.M., Valladadres, C.E., Sheehan, R., 2002. Effect of magnetic activity on the dynamics of equatorial F region irregularities. J. Geophys. Res. 107, 1489. https://doi.org/10.1029/2002J.

Chapagain, N.P., 2015. Electrodynamics of the low-latitude thermosphere by comparison of zonal neutral winds and equatorial plasma bubble velocity. Journal of Institute of Science and Technology 20 (2), 84–89.

Chapagain, N.P., Fisher, D.J., Meriwether, J.W., Chau, J.L., Makela, J.J., 2013. Comparison of zonal neutral winds with equatorial plasma bubble and plasma drift velocities. J. Geophys. Res. Space Physics 118, 1802–1812. https://doi.org/10.1002/jgra.50238.

Chapagain, N.P., Makela, J.J., Meriwether, J.W., Fisher, D.J., Buriti, R.A., Medeiros, A.F., 2012. Comparison of nighttime zonal neutral winds and equatorial plasma bubble drift velocities over Brazil. J. Geophys. Res. 117, A06309. https://doi.org/10.1029/2012JA017620.

Chen, C.H., Lin, C., Chen, W.H., Matsuo, T., 2017. Modeling the ionospheric prereversal enhancement by using coupled thermosphere-ionosphere data assimilation. Geophys. Res. Lett. 44, 1652–1659. https://doi.org/10.1002/2016GL071812.

Conde, M., Craven, J.D., Immel, T., Hoch, E., Stenbaek-Nielsen, H., Hallinan, T., Smith, R.W., Olson, J., Wei, S., 2001. Assimilated observations of thermospheric winds, the aurora, and ionospheric currents over Alaska. J. Geophys. Res. 106 (A6), 10493–10508. https://doi.org/10.1029/2000JA000135.

de Paula, E.R., de Oliveira, C.B.A., Caton, R.G., et al., 2019. Ionospheric irregularity behavior during the September 6–10, 2017 magnetic storm over Brazilian equatorial–low latitudes. Earth Planets Space 71 (42). https://doi.org/10.1186/s40623-019-1020-z.

Fagundes, P.R., Sahai, Y., Bittencourt, J.A., Takahashi, H., 1996. Plasma drifts inferred from thermospheric neutral winds and temperature gradients observed at low latitudes. J. Atmos. Terr. Phys. 58 (11), 1219–1228.

Fejer, B.G., Scherliess, L., 1998. Mid-and low-latitude prompt-penetration ionospheric zonal plasma drifts. Geophys. Res. Lett. 25 (16), 3071–3074. https://doi.org/10.1029/98GL02325.

Fukushima, D., Shiokawa, K., Otsuka, Y., Nishioka, M., Kubota, M., Tsugawa, T., Nagatsuma, T., Komonjinda, S., Yatini, C.Y., 2015. Geomagnetically conjugate observation of plasma bubbles and thermospheric neutral winds at low latitudes. J. Geophys. Res. Space Physics 120. https://doi.org/10.1002/2014JA020398.

Huang, C.S., Foster, J.C., Kelley, M.C., 2005. Long-duration penetration of the interplanetary electric field to the low-latitude ionosphere during the main phase of magnetic storms. J. Geophys. Res. 110, A11309. https://doi.org/10.1029/2005JA011202.

Huang, C.S., Rich, F.J., Burke, W.J., 2010. Storm time electric fields in the equatorial ionosphere observed near the dusk meridian. J. Geophys. Res. 115, A08313. https://doi.org/10.1029/2009JA015150.

Huang, C.S., Roddy, P.A., 2016. Effects of solar and geomagnetic activities on the zonal drift of equatorial plasma bubbles. J. Geophys. Res. 121, 628–637. https://doi.org/10.1002/2015JA021900.

Kelley, M.C., 1989. The Earth's Ionosphere. Academic, San Diego, CA.

Kikuchi, T., Luhr, H., Schlegel, K., Tachihara, H., Shinohara, M., Kitamura, T.L., 2000. Penetration of auroral electric fields to the equator during a substorm. J. Geophys. Res. 105, 23251–23252.

Koucka, K.P., Podolska, K., Potuznikova, K., Kouba, D., Mosna, Z., Boska, J., Kozubek, M., 2020. Evidence of vertical coupling: meteorological storm Fabienne on 23 September 2018 and its related effects observed up to the ionosphere. Ann. Geophys. 38, 73–93. https://doi.org/10.5194/angeo-38-73-2020.

Makela, J.J., Meriwether, J.W., Huang, Y., Sherwood, P.J., 2011. Simulation and analysis of a multi-order imaging Fabry-Perot interferometer for the study of thermospheric winds and temperatures. Appl. Opt. 50 (22), 4403.

Maute, A., Richmond, A.D., 2017. F-region dynamo simulations at low and mid-latitude. Space Sci. Rev. 206, 471–493. https://doi.org/10.1007/s11214-016-0262-3.

Nishida, A., 1968. Coherence of geomagnetic DP 2 fluctuations with interplanetary magnetic variations. J. Geophys. Res. 73, 5549–5559. https://doi.org/10.1029/JA073i017p05549.

Oberheide, J., Shiokawa, K., Gurubaran, S., et al., 2015. The geospace response to variable inputs from the lower atmosphere: a review of the progress made by Task Group 4 of CAWSES-II. Prog. in Earth and Planet. Sci. 2 (2) https://doi.org/10.1186/s40645-014-0031-4.

Okoh, D., Rabiu, B., Shiokawa, K., Otsuka, Y., Segun, B., Falayi, E., Onwuneme, S., Kaka, R., 2017. First study on the occurrence frequency of equatorial plasma bubbles over West Africa using an all-sky airglow imager and GNSS receivers. J. Geophys. Res. Space Phys. 122, 12430–12444. https://doi.org/10.1002/2017JA024602.

Park, J., Lühr, H., Min, K.W., 2010. Characteristics of F-region dynamo currents deduced from CHAMP magnetic field measurements. J. Geophys. Res. 115, A10302. https://doi.org/10.1029/2010JA015604.

Rishbeth, H., 1971a. The F-layer dynamo. Planet. Space Sci. 19 (2), 263–267.

Rishbeth, H., 1971b. Polarization fields produced by winds in the equatorial F-region. Planet. Space Sci. 19 (3), 357–369. https://doi.org/10.1016/0032-0633(71)90098-5.

Rishbeth, H., 2000. The equatorial F layer: progress and puzzles. Ann. Geophys. 18, 730–739.

Santos, A.M., Abdu, M.A., Souza, J.R., Sobral, J.H.A., Batista, I.S., Denardini, C.M., 2016. Storm time equatorial plasma bubble zonal drift reversal due to disturbance Hall electric field over the Brazilian region. J. Geophys. Res. Space Phys. 121, 5594–5612. https://doi.org/10.1002/2015JA022179.

Sarudin, I., Hamid, N., Abdullah, M., Buhari, M., 2019. Comparison of equatorial plasma bubble zonal drifts and neutral winds velocity over Southeast Asia. IOP Conf. Series: J. Phys. Conf. 1152, 012014 https://doi.org/10.1088/1742-6596/1152/1/012014.

Schunk, R.W., Sojka, J.J., 1996. Ionosphere-thermosphere space weather issues. J. Atmos. Terr. Phys. 58 (14), 1527–1574.

Shiokawa, K., Otsuka, Y., Oyama, S., Nozawa, S., Satoh, M., Katoh, Y., Hamaguchi, Y., Yamamoto, Y., Meriwether, J.W., 2012. Development of low-cost sky-scanning Fabry-Perot interferometer for airglow and auroral studies Earth. Planets and Space 64, 1033–1046. https://doi.org/10.5047/eps.2012.05.004.

Shiokawa, K., Otsuka, Y., Ogawa, T., 2009. Propagation characteristics of nighttime mesospheric and thermospheric waves observed by optical mesosphere thermosphere imagers at middle and low latitudes. Earth Planets Space 61, 479–491. https://doi.org/10.1186/BF03353165.

Sivakandan, M., Paulino, I., Ramkumar, T.K., Taori, A., Patra, A.K., Sripathi, S., Niranjan, K., Bilibio, A.V., 2019. Multi-instrument investigation of troposphere-ionosphere coupling and the role of gravity waves in the formation of equatorial plasma bubble. J. Atmos. Sol. Terr. Phys. 189, 65–79.

Sripathi, S., Abdu, M.A., Patra, A.K., Ghodpage, R.N., 2018. Unusual generation of localized EPB in the dawn sector triggered by a moderate geomagnetic storm. J. Geophys. Res.: Space Physics 123, 9697–9710. https://doi.org/10.1029/2018JA025642.

Tesema, F., Mesquita, R., Meriwether, J., Damtie, B., Nigussie, M., Makela, J., Fisher, D., Harding, B., Yizengaw, E., Sanders, S., 2017. New results on equatorial thermospheric winds and temperatures from Ethiopia, Africa. Ann. Geophys. 35, 333–344. https://doi.org/10.5194/angeo-35-333-2017.

Tulasi Ram, S., Yokoyama, T., Otsuka, Y., Shiokawa, K., Sripathi, S., Veenadhari, B., Heelis, R., Ajith, K.K., Gowtam, V.S., Gurubaran, S., Supnithi, P., Le Huy, M., et al., 2015. Duskside enhancement of equatorial zonal electric field response to convection electric fields during the St. Patrick's Day storm on 17 March 2015. J. Geophys. Res. Space Physics 120. https://doi.org/10.1002/2015JA021932.

Wiens, R.H., Ledvina, B.M., Kintner, P.M., Afewerki, M., Mulugheta, Z., 2006. Equatorial plasma bubbles in the ionosphere over Eritrea: occurrence and drift speed. Ann. Geophys. 24 (5), 1443–1453. https://doi.org/10.5194/angeo-24-1443-2006.

Wu, Q., Gablehouse, R.D., Solomon, S.C., Killeen, T.L., She, C.Y., 2004. A new Fabry-Perot interferometer for upper atmosphere research. Proc. SPIE 5660, Instruments, Science, and Methods for Geospace and Planetary Remote Sensing. https://doi.org/10.1117/12.573084, 30 December 2004.

Xu, H., Shiokawa, K., Oyama, S., et al., 2019. Thermospheric wind variations observed by a Fabry–Perot interferometer at Tromsø, Norway, at substorm onsets. Earth Planets Space 71 (93). https://doi.org/10.1186/s40623-019-1072-0.

Yigit, E., Knizova, P.K., Georgieva, K., Ward, W., 2016. A review of vertical coupling in the Atmosphere–Ionosphere system: effects of waves, sudden stratospheric warmings, space weather, and of solar activity. J. Atmos. Sol. Terr. Phys. 141, 1–12.